Title	A model for hybrid simulations of molecular dynamics and computational fluid dynamics
Author(s)	Yasuda, Shugo; Yamamoto, Ryoichi
Citation	PHYSICS OF FLUIDS (2008), 20(11)
Issue Date	2008-11
URL	http://hdl.handle.net/2433/84565
Right	Copyright 2008 American Institute of Physics. This article may be downloaded for personal use only. Any other use requires prior permission of the author and the American Institute of Physics.
Type	Journal Article
Textversion	publisher

A model for hybrid simulations of molecular dynamics and computational fluid dynamics

Shugo Yasuda[a] and Ryoichi Yamamoto[b]
Department of Chemical Engineering, Kyoto University, Kyoto 615-8510, Japan
and CREST, Japan Science and Technology Agency, Kawaguchi 332-0012, Japan

(Received 15 March 2008; accepted 29 September 2008; published online 6 November 2008)

We develop a method for multiscale hybrid simulations of molecular dynamics (MD) and computational fluid dynamics (CFD). In this method, the usual lattice-mesh based simulations are applied for the CFD level, but each lattice is associated with a small MD cell that generates a "local stress" according to a "local flow field" given from CFD instead of using any constitutive functions at the CFD level. We carried out hybrid simulations for some elemental flow problems involving simple Lennard-Jones liquids and compared the results with those obtained by usual CFD with a Newtonian constitutive relation in order to examine the validity of our hybrid simulation method. It is demonstrated that our hybrid simulations successfully reproduce the correct flow behavior obtained from usual CFD as long as the mesh size Δx and the time step Δt of CFD are not too large compared to the system size l_{MD} and the sampling duration t_{MD} of MD simulations performed at each time step of the CFD. Otherwise, the simulations are affected by large fluctuations due to poor statistical averages taken in the MD part. Properties of the fluctuations are analyzed in detail.
 [DOI: 10.1063/1.3003218]

I. INTRODUCTION

The hydrodynamics of complex fluids are of particular importance in various science and engineering fields, such as fluid mechanics, soft matter science, mechanical engineering, and chemical engineering. Due to the complicated couplings between the internal degrees of freedom of complex fluids and their flow behavior, conventional treatments, based on the usual assumptions such as the nonslip boundary condition and the linear-Newtonian constitutive relation, are often invalid. Striking examples can be seen in systems such as colloidal dispersions, polymeric liquids, granular matters, and liquid crystals. Those systems are known to exhibit peculiar flow behaviors, e.g., shear thinning or thickening, viscoelasticity, jamming, and flow induced phase transition.

Although there exists a huge accumulation of experimental and theoretical studies on the rheology of complex fluids, performing computational fluid dynamics (CFD) simulations is not yet common for complex fluids since reliable constitutive equations are often unknown for those systems. On the other hand, there also exists a different problem for microscopic approaches such as molecular dynamics (MD) simulations, although constitutive equations are no longer necessary in this case. The characteristic time and length scales of complex fluids easily become several orders larger than those of microscopic scales. Therefore, most hydrodynamic problems of complex fluids are still out of reach of microscopic MD simulations. To overcome the serious limitations mentioned above, we aim to develop a new multiscale method for performing hybrid simulations of MD and CFD valid for complex fluids without any constitutive equations.

Various methods for hybrid simulations of MD and CFD have already been proposed by several researchers. Most of those methods are based on "domain decomposition" for which MD simulations are applied only around the points of interest, i.e., in the vicinity of defects, boundaries, and interfaces, where details of molecular motions are important, while the remaining regions are treated only by CFD.[1–10] The exchange of information between MD and CFD is performed in coupling regions where the two systems are constrained to be consistent. This kind of hybrid method is expected to be useful especially for problems involving interfaces, such as adhesion, friction, anchoring of liquid crystals, and stick-slip motions.

In order to apply hybrid methods of MD and CFD to the hydrodynamics of complex fluids, a different type of approach is probably needed. Our strategy for this is straightforward. We try to develop a multiscale hybrid method based on a local sampling concept. Here, CFD is used as a fluid solver, while nonequilibrium MD simulations are used to generate local properties by performing local statistical sampling in a consistent manner. The numerical algorithm is rather simple. We perform usual lattice-mesh based CFD simulations at an upper level, but each mesh node is associated with a small lower level MD cell that provides a "local stress" to the CFD level according to a "local flow field" passed from CFD to the MD level instead of using any constitutive functions at the CFD level. Nonequilibrium MD simulations thus have to be performed at all node points and at every time step of CFD.

One might think that the simulations would be much faster if we construct a tabular database of the constitutive relations by performing MD simulations in advance under

[a]Electronic mail: yasuda@cheme.kyoto-u.ac.jp.
[b]Electronic mail: ryoichi@cheme.kyoto-u.ac.jp.

many different simulation parameters and refer to the table from CFD. The "tabular approach" works effectively for simple fluids for which the constitutive relations depend only on a few parameters, such as the density, temperature, and shear rate. In the case of complex fluids, however, the number of parameters to be considered can be huge depending on the local quantities to be considered. In the case of charged systems, for example, the local stress depends on the local compositions and chemical potentials of ions and the local electric field, etc. Although we used only a simple Lennard-Jones (LJ) liquid in the present study, we adopt the local sampling strategy rather than the tabular contraction strategy to be more general. The main purpose of the present study is to examine the validity of our multiscale hybrid model by performing some simple demonstrations of the method. The efficiency and drawbacks of both strategies will be considered in the future for more specific problems. To clarify the validity of our hybrid method, we solely treat the elemental flows of the simple LJ liquids with the nonslip boundary condition and compare the results with those obtained by usual CFD for the incompressible Navier–Stokes equations. An extension to treat interface problems and non-Newtonian complex flows will also be implemented in the future.

The basic ideas to implement the present method were put forward earlier by Kevrekidis *et al.*[11] and also by Ren and E.[12] In Ref. 11, the equation-free multiscale approach is proposed, in which macroscopic evolutions are computed directly from the microscopic simulations without using any equations at the macroscopic level. In Ref. 12, the heterogeneous multiscale method (HMM) for complex liquids is proposed for both bulk and boundary problems. The present hybrid method may be categorized as the HMM type.[13] In the present method, however, the actual implementations of the CFD-MD coupling scheme is modified from that proposed in Ref. 12. The modifications are explained in Sec. II B and also in Sec. V.

The hybrid simulation method is described in Sec. II, and some demonstrative results for one-dimensional (1D) and two-dimensional (2D) flows of simple LJ liquids are shown in Sec. III. Special attention is given to the efficiency and the reliability of our hybrid method there. The simulation results obtained by our multiscale hybrid method are compared with those of normal CFD with the Newtonian constitutive relation. The validity of our method is discussed in Sec. IV, and a summary is given in Sec. V.

II. HYBRID MODEL

Incompressible flows for isotropic materials are described by the following equations:

$$\frac{\partial v_\alpha}{\partial x_\alpha} = 0, \tag{1}$$

$$\frac{\partial v_\alpha}{\partial t} + v_\beta \frac{\partial v_\alpha}{\partial x_\beta} = \frac{1}{\rho}\frac{\partial P_{\alpha\beta}}{\partial x_\beta} + g_\alpha, \tag{2}$$

where x_α is the Cartesian coordinate system, t the time, v_α the velocity, ρ the density, $P_{\alpha\beta}$ the stress tensor, and g_α the external force per unit mass. Here and afterwards, the subscripts α, β, and γ represent the index in Cartesian coordinates, i.e., $\{\alpha,\beta,\gamma\}=\{x,y,z\}$, and the summation convention is used. The stress tensor $P_{\alpha\beta}$ is written in the form

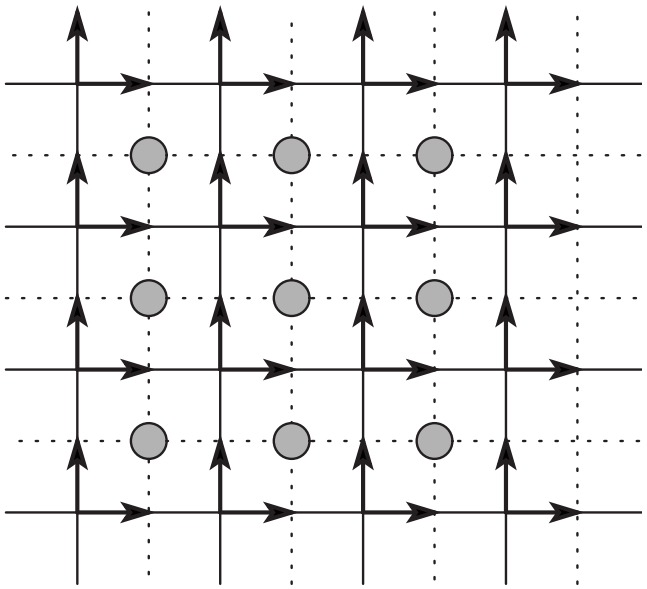

FIG. 1. Staggered arrangement of vector quantity, the velocity $\boldsymbol{v}$, and a scalar quantity, the pressure p and density ρ, on a lattice-mesh grid.

$$P_{\alpha\beta} = -p\delta_{\alpha\beta} + T_{\alpha\beta}, \tag{3}$$

where p is the pressure and $\delta_{\alpha\beta}$ is the Kronecker delta. Here we assumed that the diagonal component of the stress tensor is isotropic. The off-diagonal stress tensor is symmetric, $T_{\alpha\beta}=T_{\beta\alpha}$, and traceless, $T_{\alpha\alpha}=0$.[14] In order to solve the above equations, one needs a constitutive relation for the stress tensor $T_{\alpha\beta}$. In our hybrid method, instead of using any explicit formula such as the Newtonian constitutive relation, $T_{\alpha\beta}$ is computed directly by MD simulations.

A. CFD scheme

We use a lattice-mesh based finite volume method with a staggered arrangement for vector and scalar quantities[15] (see Fig. 1). The control volume for a vector quantity is a unit square surrounded by dashed lines, and that for a scalar quantity is a unit square surrounded by solid lines. Equations (1) and (2) are discretized by integrating the quantities on each control volume. As for numerical time integrations, we use the fourth order Runge–Kutta method, where a single physical time step Δt is divided into four substeps. More concretely, the time evolution of a quantity, ϕ, which is to be determined by the equation $\partial\phi/\partial t = f(t,\phi)$, is written as

$$\phi^*_{n+1/2} = \phi^n + \frac{\Delta t}{2} f(t_n, \phi^n), \tag{4a}$$

$$\phi^{**}_{n+1/2} = \phi^n + \frac{\Delta t}{2} f(t_{n+1/2}, \phi^*_{n+1/2}), \tag{4b}$$

$$\phi^*_{n+1} = \phi^n + \Delta t f(t_{n+1/2}, \phi^{**}_{n+1/2}), \tag{4c}$$

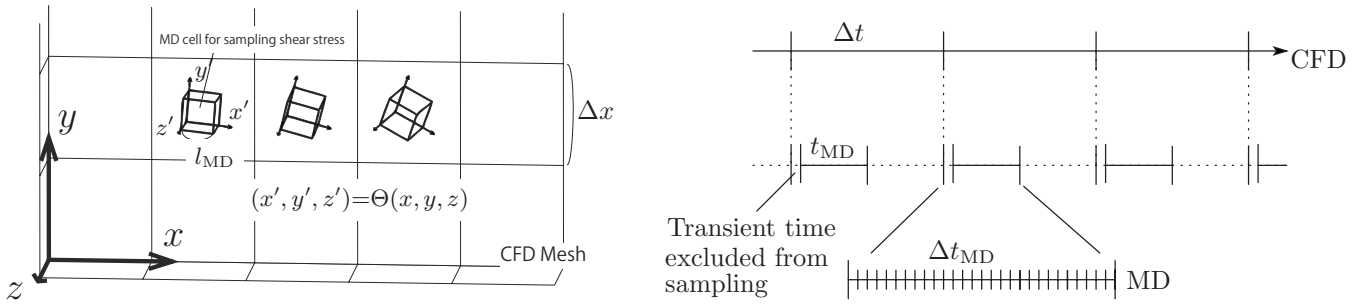

(a) Space decomposition (b) Time evolution

FIG. 2. Schematic for the hybrid scheme. (a) CFD simulations are performed in a reference coordinate (x,y,z), while MD simulations are performed in a rotated coordinate (x',y',z') so that the diagonal components of $E'_{\alpha\beta}$ all become zero with the procedure described in Sec. II B. The CFD system is discretized into cubic subsystems whose side length is Δx. Each subsystem is associated with a MD cell, whose side length is l_{MD}, with Lees–Edward periodic boundary condition under shear deformation. Note that three-dimensional MD simulations are used at the microscopic level even for the problems that 1D or 2D analysis is applied at the macroscopic level. (b) A schematic time evolution of our multiscale method. The CFD simulation proceeds with a time step of Δt, and the MD simulation is carried out for a lapse of time t_{MD} only to sample the local stress $T'_{\alpha\beta}$ at each node point and time step of CFD.

$$\phi^{n+1} = \phi^n + \frac{\Delta t}{6}[f(t_n,\phi^n) + 2f(t_{n+1/2},\phi^*_{n+1/2}) + 2f(t_{n+1/2},\phi^{**}_{n+1/2}) + f(t_{n+1},\phi^*_{n+1})]. \tag{4d}$$

The time evolution of the fluid velocity $\boldsymbol{v}$ is computed by the above set of equations. On the other hand, the pressure p is determined so that the fluid velocity satisfies incompressible condition (1) at each substep. The procedure at each substep is written as

$$p = \tilde{p} + \psi, \tag{5a}$$

$$\boldsymbol{v} = \tilde{\boldsymbol{v}} - \tau \nabla \psi, \tag{5b}$$

$$\Delta\psi = \frac{1}{\tau}\nabla\tilde{\boldsymbol{v}}, \tag{5c}$$

where $\tilde{p}$ is the pressure obtained at the previous substep, $\tilde{\boldsymbol{v}}$ is the velocity obtained by solving Eq. (4) at the present substep, τ is the time increment of the substep, and ψ is the correction term to obtain the divergence-free velocities. The remaining three components of the tensor $T_{\alpha\beta}$ are to be computed directly by MD simulations. The details of the method are described in Sec. II B. Note that the calculation of $T_{\alpha\beta}$ is carried out at each substep of Eq. (4).

B. Computation of local stress by MD

We compute the local stresses by MD simulations according to the local strain rates, rather than the local flow velocities themselves, computed at the CFD level. A schematic of the method is depicted in Fig. 2. At the CFD level, the local strain rate tensor $E_{\alpha\beta}$ is defined as

$$E_{\alpha\beta} = \frac{1}{2}\left(\frac{\partial v_\alpha}{\partial x_\beta} + \frac{\partial v_\beta}{\partial x_\alpha}\right), \tag{6}$$

where the incompressible condition, $E_{\alpha\alpha}=0$, is to be satisfied. We can now define a rotation matrix Θ by which the strain rate tensor $E_{\alpha\beta}$ is transformed to

$$E' = \Theta E \Theta^{\mathrm{T}} = \begin{pmatrix} 0 & E'_{xy} & E'_{xz} \\ E'_{yx} & 0 & E'_{yz} \\ E'_{zx} & E'_{zy} & 0 \end{pmatrix}, \tag{7}$$

where the diagonal components all vanish. This transformation makes performing MD simulations much easier with the usual Lees–Edwards periodic boundary condition for simple shear flows under the assumption that each off-diagonal component of the local stress tensors depends only on the corresponding component of the local strain rate tensors, respectively. The off-diagonal stress tensor $T'_{\alpha\beta}$ is computed according to $E'_{\alpha\beta}$ and then passed to CFD after transforming back to the original coordinates, $T_{\alpha\beta}$. For 1D or 2D flows ($\partial/\partial z=0$ and $v_z=0$), Θ and E' are expressed as

$$\Theta = \begin{pmatrix} \cos\theta & \sin\theta \\ -\sin\theta & \cos\theta \end{pmatrix}, \tag{8}$$

$$E'_{xy} = E'_{yx} = -E_{xx}\sin 2\theta + E_{xy}\cos 2\theta, \tag{9}$$

where

$$\theta = \frac{1}{2}\tan^{-1}\left(-\frac{E_{xx}}{E_{xy}}\right). \tag{10}$$

Nonequilibrium MD simulations for simple shear flows in the rotated Cartesian coordinates are performed in many MD cells according to the local strain rate E' defined at each lattice node of the CFD. The number of particles in each MD cell is 256 if explicitly stated. Once a local stress tensor $P'_{\alpha\beta}$ is obtained at the MD level, the local stress at each lattice node $P_{\alpha\beta}$ in the original coordinate system is obtained by combining the pressure p obtained *a priori* by CFD and a tensor $T'_{\alpha\beta}$ obtained by subtracting the isotropic normal stress components from $P'_{\alpha\beta}$ as

$$P = \Theta^T[-pI + T']\Theta = -pI + \Theta^T T'\Theta, \tag{11}$$

where I is the unit tensor. For 1D or 2D flows, we can use $T'_{xx}=T'_{yy}=0$ and $T'_{xy}=T'_{yx}=P'_{xy}$.

TABLE I. Simulation parameters.

	l^*_{MD}	t^*_{MD}	L^*	U^*	Re	$\Delta x/l_{MD}$	$\Delta t/t_{MD}$
			1D channel flow				
SP I	6.84	1.87	116	4.30	200	1.0	1.0
SP II	6.84	3.74	233	2.15	200	2.0	2.0
SP III	6.84	7.49	465	1.08	200	4.0	4.0
			2D channel flow				
SP IV	6.84	3.74	233	2.15	200	2.0	2.0
			2D cavity flow				
SP V	6.84	4.68	219	0.46	59	1.0	1.0
SP VI	6.84	9.36	438	0.91	235	2.0	2.0
SP VII	6.84	3.11	876	1.83	941	4.0	4.0
SP VIII	8.62	9.36	438	0.91	235	1.59	2.0
SP IX	8.62	18.7	438	0.91	235	1.59	1.0

In the nonequilibrium MD simulations, we use the Lees–Edwards sheared periodic boundary condition for cubic MD. The temperature is kept constant by using the Gaussian isokinetic thermostat.[16–19] The density is also fixed in each MD simulation by the number of particles and the box size. Thus, we calculate the local stress with the so-called *NVT* ensembles, $P'(\rho,T,E')$. The stress is averaged in steady states after transient behavior has vanished. In the present computations, the transient time in each MD process is set as one-tenth of the CFD time step, $\Delta t/10$. The initial states in each MD simulation are created by rescaling the thermal velocities of molecules to be fixed to the local temperatures without changing the molecular configurations from those obtained by the previous process.

III. NUMERICAL COMPUTATION

We have carried out the hybrid simulations for 1D and 2D flows of a simple liquid composed of LJ particles interacting via the potential

$$v^{\mathrm{LJ}}(r) = 4\varepsilon\left[\left(\frac{\sigma}{r}\right)^{12} - \left(\frac{\sigma}{r}\right)^{6}\right]. \tag{12}$$

In the present simulations, the potential is truncated at $r=r_c$ and shifted to zero at the distance for computational efficiency. We considered only the cases where the temperature T and the fluid density ρ are uniform and constant over the CFD systems and the external force is neglected, $g_\alpha=0$. The reduced temperature $T^*=Tk/\varepsilon$ and reduced density $\rho^*=\rho\sigma^3/m$, where k is the Boltzmann constant and m is the mass of a single LJ particle, are fixed at $T^*=1.0$ and $\rho^*=0.8$ in the simulations. Hereafter, nondimensional quantities normalized by the energy and length parameters of the LJ potential, ε and σ, and the mass of molecule, m, are denoted by the superscript "$*$."

In the following, Δt and Δx represent the time step and the mesh size of CFD calculations, and t_{MD} and l_{MD} represent the sampling duration and the side length of a MD cell, respectively. The two parameters $\Delta t/t_{MD}$ and $\Delta x/l_{MD}$ represent the efficiency of our hybrid simulations. We have carried out hybrid simulations with several different values of the parameters and compared the results with those obtained by usual CFD. In the present simulations we fix the time-step size of the MD simulation Δt_{MD} as $\Delta t^*_{MD}=0.005$. The values of l_{MD}, t_{MD}, Δx, and Δt can be found in Table I. We note that the sampling durations of the MD simulation, t_{MD}, are set to be larger than the correlation time of the temporal shear stress for the bulk fluids ($\sim$0.1 for normal liquids) which can be measured in equilibrium MD simulations. The time-step size of CFD, Δt, is set to be small enough for the CFD solutions to be stable.

A. Pressure-driven channel flows

The LJ liquid with $r^*_c=2.5$ is contained in a channel composed of two parallel plates located at $x_1=\pm L/2$ and subjected to a pressure gradient in the y direction. We performed 1D and 2D simulations for these pressure-driven channel flows. The pressure difference over a distance L, Δp, is set as $\Delta p/\rho U^2=0.05$, where U is a characteristic flow velocity. The values of characteristic length L and velocity U in terms of the LJ units can be referred in Table I. A nonslip boundary condition is applied on the two plates.

The results of 1D simulations are shown in Figs. 3 and 4. A symmetric condition is used at $x=0$, and the computational domain $[-L/2,0]$ is divided into eight slits. The parameters used in the simulations are listed as SP I–SP III in Table I. In the corresponding CFD simulation, viscosity is set as $\eta^*=2.0$, which is for the LJ liquid with $r^*_c=2.5$ at $T^*=1.0$ and $\rho^*=0.8$. The Reynolds number defined as $\rho UL/\eta$ is fixed at 200. It is seen in Fig. 3 that the results obtained by the present hybrid simulations agree well with those from usual CFD for the case $\Delta t/t_{MD}\leq 2$ and $\Delta x/l_{MD}\leq 2$. When the parameters become large, instantaneous velocity profiles tend to fluctuate as seen in Fig. 4. It should be noted that the fluctuations can be removed by taking time averages. This means that the mean value of the fluctuation is almost zero, i.e., the fluctuation might also be removed by applying some

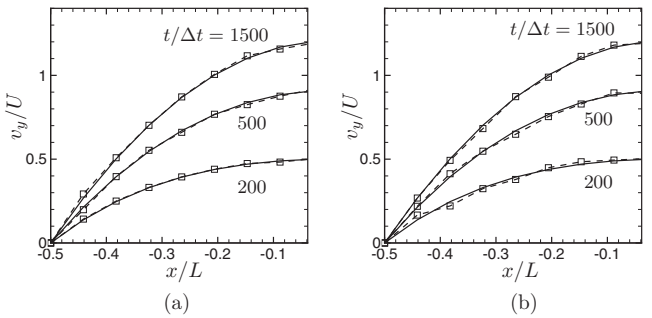

FIG. 3. The velocity profiles obtained by 1D computations for the pressure-driven channel flow. Simulation parameters are summarized as SP I in Table I for (a) and SP II in Table I for (b). Time evolutions of the velocity profile after an application of pressure gradient in the y direction at $t=0$. The solid lines show the results of the usual CFD simulation, and the dotted lines and square symbols show the results of the present hybrid simulation.

filtering, etc. The fractional root-mean-square (rms) deviations of the results of the hybrid simulations away from the results of CFD are shown in Table II.

The results of 2D simulations are shown in Fig. 5. The computational domain is now $[-L/2,L/2]\times[0,L/2]$ and divided into 16×8 uniform lattices. A nonslip boundary condition is used at $x=\pm L/2$. At $y=0$ and $L/2$, a periodic condition is used for the velocity, and the pressure is set to $p(x,L/2)=p(x,0)-0.5\Delta p$. It is seen that fluctuations in an instantaneous profile of the velocity are much smaller than fluctuations in the pressure. This is clearly due to the incompressibility condition imposed on the velocity. The velocity also fluctuates immediately after solving Eq. (2); however, the incompressibility condition Eq. (1) tends to adjust it. The pressure fluctuations can also be removed by taking time averages. It is seen from Table II that the rms deviation is almost the same as that in the case of a 1D computation with the same values of the ratios $\Delta x/l_{\mathrm{MD}}$ and $\Delta t/t_{\mathrm{MD}}$. See SP II and SP IV in Table II.

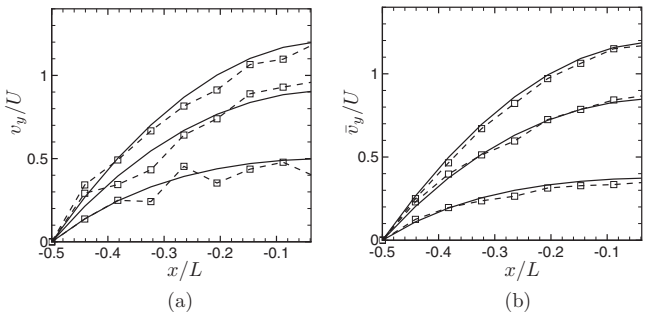

FIG. 4. The velocity profiles obtained by 1D computations for the pressure-driven channel flow. Simulation parameters are summarized as SP III in Table I. Time evolutions of the velocity profile after an application of pressure gradient in the y direction at $t=0$. Instantaneous profiles at $t/\Delta t=200$, 500, and 1500 are shown in (a), while the velocity profiles are time averaged over $t/\Delta t=[0,300]$, $[300,600]$, and $[1200,1500]$ in (b). The squares show results of the hybrid simulations, and the dotted lines present the corresponding CFD results for comparison.

TABLE II. Fractional rms deviations, which are defined as $\sqrt{\int_0^L dx^d \int_0^T dt(Q-Q_{\mathrm{NS}})^2/L^d T}/\max|Q_{\mathrm{NS}}|$ for the velocity ($Q=\boldsymbol{v}$) and for the shear stress ($Q=P_{xy}$). Here d is the number of space dimensions in CFD.

	rms deviation	
	$\mathbf{v}$	P_{xy}
SP I	0.006	0.24
SP II	0.014	0.66
SP III	0.042	1.86
SP IV	0.014	0.66
SP V	0.049	0.36
SP VI	0.043	0.25
SP VII	0.024	0.40
SP VIII	0.036	0.17
SP IX	0.032	0.13

B. Two-dimensional cavity flows

A LJ liquid with $r_c^*=2^{1/6}$ is contained in a square box whose side length is L. At $t=0$, the upper wall starts to move from left to right at a velocity $v_w=U$. A nonslip boundary condition is applied at each wall; $v_x=U$ and $v_y=0$ at $y=L$, and $v_x=v_y=0$ at other walls. At the left- and right-upper corners, $v_x=U$ and $v_y=0$ are applied. In this problem, the nonslip condition causes singularities in the strain rates and stresses at the upper corners in the continuum description. Hence, the atomistic approach at the corners becomes important, for example, in estimating the forces on the walls.[6,20] In the present paper, however, we are developing a hybrid simulation method for the macroscopic behaviors of the bulk fluids in the global region. Thus, we use the conventional nonslip boundary condition even at the corners, so as to compare the results to those obtained by usual CFD.

The results of the hybrid simulations are shown in Figs. 6 and 7. The computational domain is divided into 32×32 uniform lattices. The values of the parameters used in the present simulations are listed as SP V–SP VII in Table I. The Reynolds number is defined as $\rho UL/\eta$, and the viscosity of the corresponding LJ fluid is $\eta^*=1.7$.

Figure 6 shows the steady-state velocity profiles time averaged over $t/\Delta t=[950,1000]$. It is clear that our hybrid method can successfully reproduce the characteristic flow properties of cavity flows with different Reynolds numbers; the size of the vortex becomes larger as the Reynolds number increases. Figure 7 shows the time evolutions of velocity profiles for the case of $\mathrm{Re}=980$ after a sudden application of upper-wall sliding at $t=0$. Here, the results obtained by hybrid simulations are compared with those of usual CFD simulations. It is observed in both the results that a small vortex first appears at the upper-right corner and then moves gradually toward the center of the box, with the size of the vortex increasing as time passes. The agreement between hybrid simulations and CFD is very good. Our hybrid method is confirmed to reproduce successfully the time evolution, while large fluctuations are seen in the instantaneous velocity profiles. Comparisons of the instantaneous profiles of the hybrid simulation and CFD are shown in Fig. 8. The rms deviations are shown in Table II.

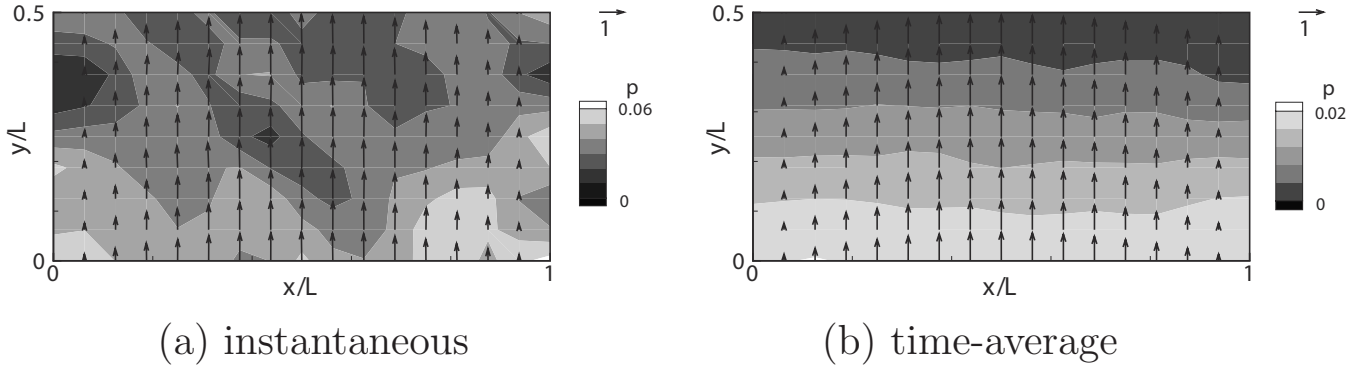

FIG. 5. Flow profiles of the pressure-driven channel flow obtained by a 2D calculation. Simulation parameters are summarized as SP IV in Table I. (a) The instantaneous profiles at $t/\Delta t=1000$. (b) The time average over $t/\Delta t=[900,1000]$.

IV. DISCUSSION

As mentioned above, the ratios $\Delta t/t_{\mathrm{MD}}$ and $\Delta x/l_{\mathrm{MD}}$ measure the efficiency of our hybrid simulations. The larger the ratios, the more efficient the simulations; however, the statistical fluctuations also become large. For example, in the case of $\Delta t/t_{\mathrm{MD}}=\Delta x/l_{\mathrm{MD}}=4$, computational efficiency is, roughly speaking, $4^D\times 4$ times more efficient than a full MD simulation of a D-dimensional cubic system. The fractional rms deviations of the results of the hybrid simulations from those of CFD are shown in Table II. The comparison between those for SP I–SP IV shows the effect of the ratios $\Delta x/l_{\mathrm{MD}}$ and $\Delta t/t_{\mathrm{MD}}$ on the rms deviations in the case that the Reynolds number is fixed. The results of the hybrid simulations show good agreement with those of CFD as far as $\Delta x/l_{\mathrm{MD}}$ and $\Delta t/t_{\mathrm{MD}}$ remain small; for the case of $\Delta x/l_{\mathrm{MD}}\leq 2$ and $\Delta t/t_{\mathrm{MD}}\leq 2$, the rms deviations are less than 0.02 for the velocity and less than 0.7 for the shear stress. As the ratios increase, the rms deviations become larger (see also Figs. 3 and 4). It is worth mentioning that the instantaneous velocity fluctuations are notable at each time step; however, they can be removed almost completely by taking time averages (see Figs. 4 and 5), although taking time averages increases the cost of the hybrid simulation and decreases its efficiency. The comparison between SP V–SP VII shows the effect of the Reynolds number on the rms deviations. Although the values of the ratios $\Delta x/l_{\mathrm{MD}}$ and $\Delta t/t_{\mathrm{MD}}$ increase in the order of SP V–SP VII, the rms deviations of the velocities become rather smaller. This fact indicates that we can carry out the hybrid simulations with high efficiency for the high Reynolds number flows. From the comparison between SP VI and SP VIII it is seen that when the number of particles in each MD box increases while fixing the system size L and characteristic velocity U, the rms deviations become smaller both for the velocity and for the shear stress. The rms deviations for the shear stresses are larger than those for the velocities for all cases. This feature is also seen from Fig. 8. The fluctuations for the strain rate and shear stress are much larger than the velocity. We note that the instantaneous fluctuations are notable, but they are also removed by taking time averages. In the following part, we will discuss the nature of the fluctuations in more detail.[21]

In order to handle the statistical noise explicitly, we rewrite Eq. (11) as

$$P=-pI+\Theta^T(T'_*+R')\Theta, \tag{13}$$

where the off-diagonal stress tensor T', which is to be determined by MD sampling, is decomposed into the nonfluctuating stress T'_* and the fluctuating random stress R' due to the thermal noise. The magnitude of each component of the random stress included in MD sampling, $\langle R'^2_{\mathrm{MD}pq}\rangle$, where p and q represent the index in Cartesian coordinates and do not follow the summation convention, should depend both on the

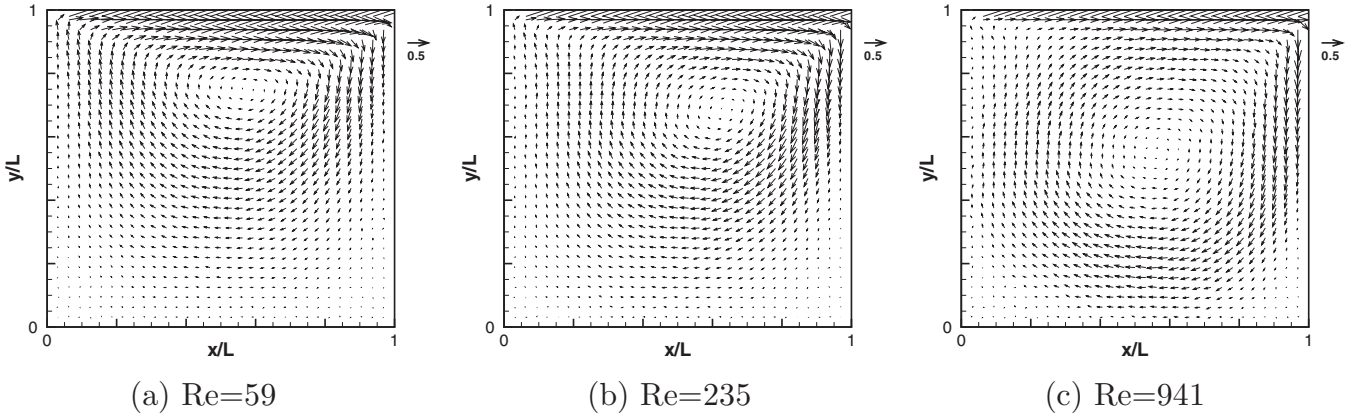

FIG. 6. The steady-state velocity profile for the cavity flow. Simulation parameters are summarized as SP V in Table I for (a), SP VI for (b), and SP VII for (c). The velocity profiles are time averaged over $t/\Delta t=[950,1000]$

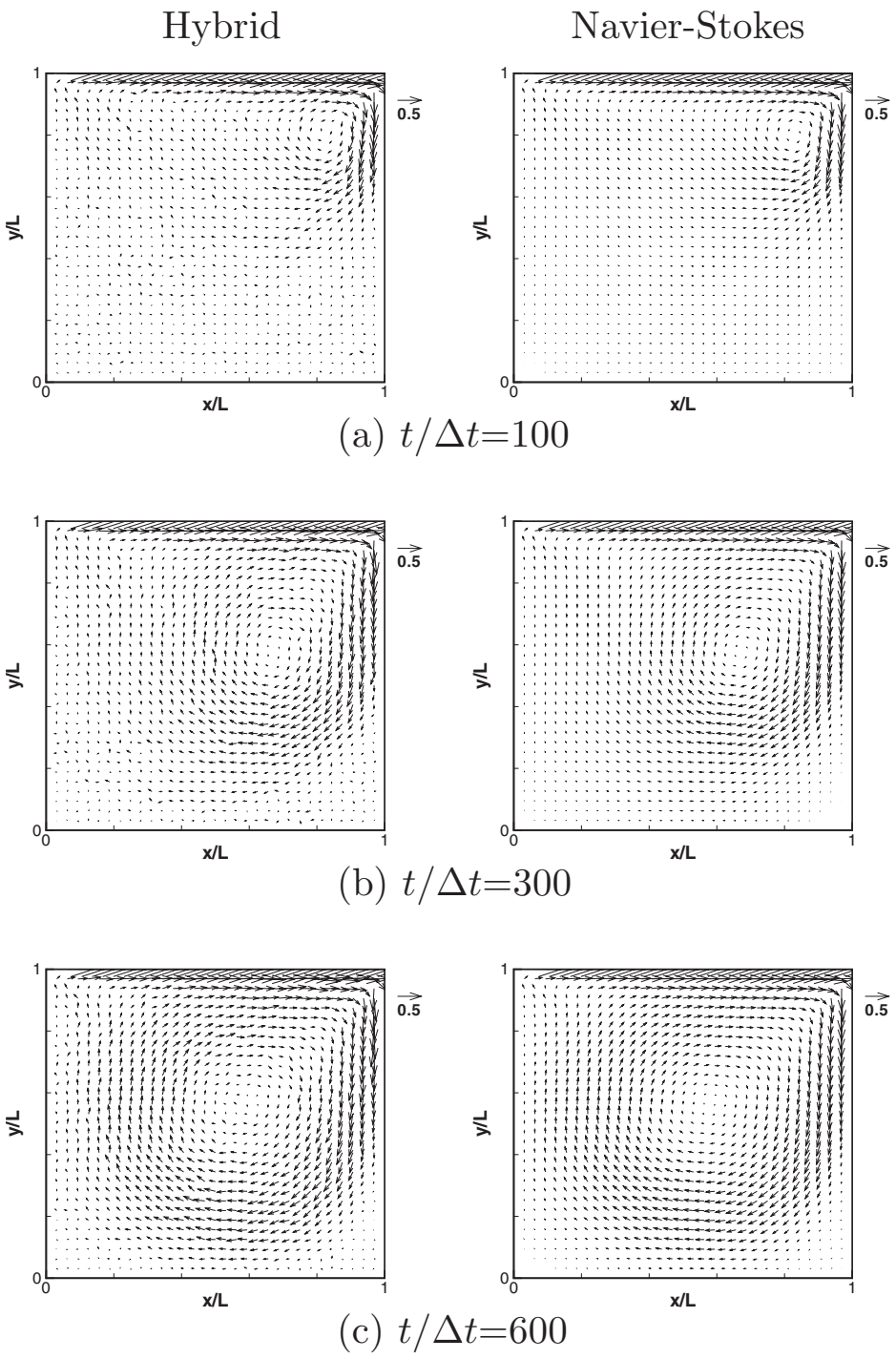

FIG. 7. Time evolutions of the velocity profile for the cavity flow with Re =980. The left column shows the hybrid simulations and the right column shows the corresponding CFD results. Simulation parameters are summarized as SP VII in Table I.

size of the MD cell, l_{MD}, and on the length of time t_{MD} over which the average is taken at the MD level, $\langle R'^2_{\mathrm{MD}pq}\rangle = \langle \bar{R}_{pq}(l_{\mathrm{MD}}, t_{\mathrm{MD}})^2\rangle$, where $\bar{R}(l,t)$ represents the random stress tensor averaged in a cubic with side length l and over a time duration t.

At the CFD level which is discretized with a mesh size Δx and a time step Δt, the physically correct magnitude should be $\langle R'^2_{\mathrm{CFD}pq}\rangle = \langle \bar{R}_{pq}(\Delta x, \Delta t)^2\rangle$. If the central limit theorem, $\langle \bar{R}_{pq}(l,t)^2\rangle \propto 1/l^D t$, is assumed, the following simple formula can be used:

$$\langle R'^2_{\mathrm{MD}pq}\rangle = \left(\frac{\Delta x}{l_{\mathrm{MD}}}\right)^D \left(\frac{\Delta t}{t_{\mathrm{MD}}}\right) \langle R'^2_{\mathrm{CFD}pq}\rangle. \tag{14}$$

This finally leads to the following very useful expression for the correctly fluctuating stress tensor P:

$$P = -pI + \Theta^T \left[T'_* + \sqrt{\left(\frac{l_{\mathrm{MD}}}{\Delta x}\right)^D \left(\frac{t_{\mathrm{MD}}}{\Delta t}\right)} R'_{\mathrm{MD}} \right] \Theta, \tag{15}$$

to be used in CFD instead of Eq. (11). This equation indicates that if we could reweight the randomly fluctuating part R' while the nonfluctuating part T'_* remains untouched, hy-

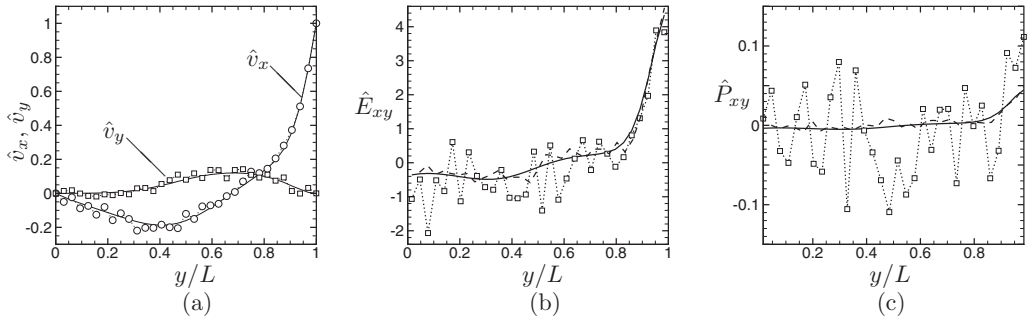

FIG. 8. Comparisons between the instantaneous profiles obtained by the hybrid simulation and those by CFD for the cavity flow for Re=235. The velocity $U\hat{v}_\alpha$, strain rate $(U/L)\hat{E}_{xy}$, and shear stress $(\rho U^2)\hat{P}_{xy}$ on the line of $x/L=0.5$ are plotted. The symbols show the results of the hybrid simulation and the solid lines those of CFD. The dashed lines in (b) and (c) show the time averages over $t/\Delta t=[900,1000]$.

drodynamic simulations including correct thermal fluctuations can be performed for complex fluids within the present framework.

We note that the important key to the development of a fluctuating hybrid simulation is the separation of T'_* and R'. We thus carried out spectral analysis for the fluctuations in the total stress tensor computed directly from MD simulations, $T'=T'_*+R'$. The discrete Fourier transformation of T'_{xy} is defined as

$$\Pi'_{xy}\{\boldsymbol{k}\}=\frac{1}{4M^2}\sum_{n_x=0}^{2M-1}\sum_{n_y=0}^{2M-1}\hat{T}'_{xy}\{\boldsymbol{x}\}\exp(-i\boldsymbol{k}\cdot\boldsymbol{x}), \tag{16}$$

where $\boldsymbol{x}=(n_x\Delta x,n_y\Delta x)$ is the position of each lattice node (n_x,n_y), $\boldsymbol{k}=(2\pi m_x/L,2\pi m_y/L)$ is the wave vector, n_x, n_y, m_z, m_y are integers, M is the lattice number in each x and y axis, and $\hat{T}'_{xy}\{\boldsymbol{x}\}$ is defined as $\hat{T}'_{xy}\{\boldsymbol{x}\}=T'_{xy}(x+\Delta x/2,y+\Delta x/2)$ for $0\le x,\ y\le L$, $\hat{T}'_{xy}\{\boldsymbol{x}\}=T'_{xy}\{2L-x,y\}$ for $L<x\le 2L$, and $\hat{T}'_{xy}\{\boldsymbol{x}\}=T'_{xy}\{x,2L-y\}$ for $L<y\le 2L$.

The power spectra $\langle|\Pi'_{xy}\{\boldsymbol{k}\}|^2\rangle$ calculated from our hybrid simulations of driven cavity flows are plotted in Fig. 9(a) for the case of $\Delta t/t_{\mathrm{MD}}=\Delta x/l_{\mathrm{MD}}=1$. This corresponds to the case of Fig. 6(a). The angular brackets $\langle\cdots\rangle$ mean the time average taken at steady state at the CFD level. One can see that the overall structure is rather simple. There exists a relatively large peak around $\boldsymbol{k}=0$ and rather flat distributions throughout the $\boldsymbol{k}$ plane. The former corresponds to the contributions from the nonfluctuating part T'_* and the latter corresponds to the contributions from the random stress R'. The same quantity obtained by conventional fluctuating hydrodynamics using a constant Newtonian viscosity and the random stress whose intensity is determined by the fluctuation-dissipation theorem[22] is shown in Fig. 9(b) for comparison.[23] Those two plots are surprisingly similar to each other including the fluctuation part. This means that our hybrid simulation generates fluctuations quite consistent with fluctuating hydrodynamics with the fluctuation-dissipation theorem in the case of $\Delta x/l_{\mathrm{MD}}=\Delta t/t_{\mathrm{MD}}=1$.

Next, one sees how the fluctuations depend on the ratios $\Delta x/l_{\mathrm{MD}}$ and $\Delta t/t_{\mathrm{MD}}$ in Fig. 10. Here, comparing to reference case (a), $(\Delta x/l_{\mathrm{MD}}=\Delta t/t_{\mathrm{MD}}=2)$, the number of particles used in MD simulations is doubled in the case of (b) $(\Delta x/l_{\mathrm{MD}}=1.59,\ \Delta t/t_{\mathrm{MD}}=2)$, and both the number of particles and the sampling duration used to take a time average are doubled in the case of (c) $(\Delta x/l_{\mathrm{MD}}=1.59,\ \Delta t/t_{\mathrm{MD}}=1)$. It is seen that the noise intensity decreases with decreasing ratios $\Delta x/l_{\mathrm{MD}}$ and $\Delta t/t_{\mathrm{MD}}$ in a way consistent with the central limiting theorem Eq. (14), i.e., the noise intensity in (b) is about one-half of that in (a), and the intensity in (c) is about one-fourth of that in (a).

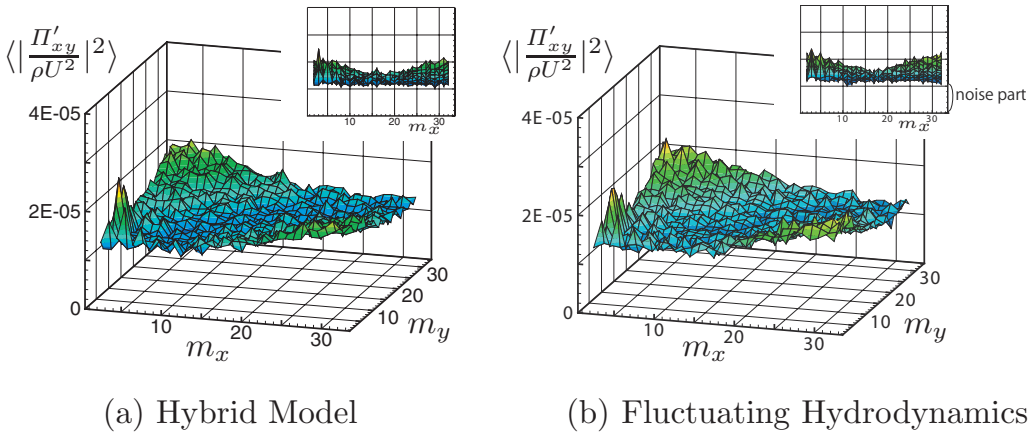

FIG. 9. (Color) The fluctuations of T'_{xy} for the case of cavity flow with Re=59. The power spectrum $\langle|\Pi'_{xy}\{\boldsymbol{k}\}|^2\rangle$ for the present multiscale model with $\Delta x/l_{\mathrm{MD}}=\Delta t/t_{\mathrm{MD}}=1$ is shown in (a) and the corresponding result from the fluctuating hydrodynamics is shown in (b) for comparison. Π'_{xy} represents the discrete Fourier transform of T'_{xy}. m_α is defined as $m_\alpha=(L/2\pi)k_\alpha$, where $\boldsymbol{k}$ is the wave vector. The insets on each figure show the $\langle|\Pi'_{xy}|^2\rangle$-$m_x$ plane.

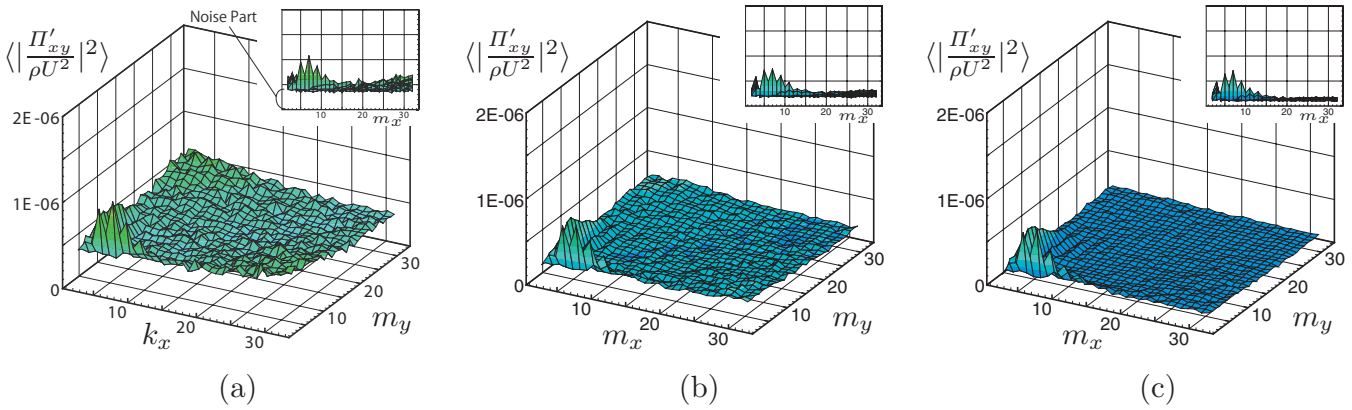

FIG. 10. (Color) The fluctuations of T'_{xy} for the case of cavity flow with Re=235. The power spectrum $\langle|\Pi'_{xy}\{\boldsymbol{k}\}|^2\rangle$ is plotted in (a) for the case of Fig. 6(b). Only the number of particles is doubled in (b), while other parameters are unchanged from (a). In (c), both the number of particles and the sampling time of T'_{xy} are doubled. Π'_{xy} represents the discrete Fourier transform of T'_{xy}. m_α is defined as $m_\alpha=(L/2\pi)k_\alpha$, where $\boldsymbol{k}$ is the wave vector. The insets in each figure show the $\langle|\Pi'_{xy}|^2\rangle$-$m_x$ plane.

From the overall properties, we can confirm that the fluctuations arising in the present hybrid simulations are white noises which obey the central limit theorem written as Eq. (14) or Eq. (15). They also indicate the possibility that some white-noise reduction algorithm, such as a low-pass filter, could be useful for the CFD-MD coupling processes.

V. SUMMARY

We develop a multiscale method for hybrid simulations of MD and CFD. The method is based on direct computations of the local stresses by performing nonequilibrium MD simulations according to the local flow field at all lattice nodes of CFD. This methodology was put forward earlier by Ren and E.[12] The present method is modified from the one proposed earlier by altering the construction of the stress tensor. In the present method, rotation matrices which transform the tensors in the Cartesian coordinates used in CFD to those convenient for MD simulations are introduced. We also replace the isotropic part of the stress tensor calculated by MD simulations with the pressure imposed by the incompressibility condition in CFD. More specifically, only the pure shear stress is passed from MD to CFD for numerical efficiency and consistency.

The validity of the method is tested by comparing the numerical results obtained by our method and usual CFD. We found that the results obtained by our hybrid method agree well with those of usual CFD with the Newtonian constitutive relation when the mesh size and the time step of CFD are not too large compared to the cell size and sampling time of MD simulations. When the ratios $\Delta t/t_{\mathrm{MD}}$ and $\Delta x/l_{\mathrm{MD}}$ become large, large fluctuations appear in the flow field of our hybrid simulations. It was, however, clarified by spectral analysis that the stress tensor T' computed by MD simulations has a very simple structure. It is composed of the nonfluctuating component T'_* and the random component R', which seem to obey a simple central limiting theorem according to the system size and the duration of the MD sampling. We confirmed that the power spectrum of the nonfluctuating component T'_* in MD sampling agrees well with that computed in usual CFD without fluctuation. The power spectrum of R' also showed good agreement with numerical results from fluctuating hydrodynamics obeying the fluctuation-dissipation theorem.

ACKNOWLEDGMENTS

The authors would like to express their gratitude to Professor Weinan E for useful discussions.

[1] S. T. O'Connell and P. A. Thompson, "Molecular dynamics–continuum hybrid computations: A tool for studying complex fluid flows," Phys. Rev. E **52**, R5792 (1995).
[2] E. G. Flekkoy, G. Wagner, and J. Feder, "Hybrid model for combined particle and continuum dynamics," Europhys. Lett. **52**, 271 (2000).
[3] R. Delgado-Buscalioni and P. V. Conveney, "Continuum-particle hybrid coupling for mass, momentum, and energy transfers in unsteady fluid flow," Phys. Rev. E **67**, 046704 (2003).
[4] R. Delgado-Buscalioni, E. G. Flekkoy, and P. V. Coveney, "Fluctuations and continuity in particle-continuum hybrid simulations of unsteady flows based on flux-exchange," Europhys. Lett. **69**, 959 (2005).
[5] X. Nie, S. Chen, W. E, and M. O. Robbins, "A continuum and molecular dynamics hybrid method for micro- and nano-fluid flow," J. Fluid Mech. **500**, 55 (2004).
[6] X. Nie, S. Chen, and M. O. Robbins, "Hybrid continuum-atomistic simulation of singular corner flow," Phys. Fluids **16**, 3579 (2004).
[7] X. Nie, M. O. Robbins, and S. Chen, "Resolving singular forces in cavity flow: Multiscale modeling from atomic to millimeter scales," Phys. Rev. Lett. **96**, 134501 (2006).
[8] J. Liu, S. Chen, X. Nie, and M. O. Robbins, "A continuum-atomistic simulation of heat transfer in micro- and nano-flows," J. Comput. Phys. **227**, 279 (2007).
[9] W. Ren, "Analytical and numerical study of coupled atomistic-continuum methods for fluids," J. Comput. Phys. **227**, 1353 (2007).
[10] T. H. Yen, C. Y. Soong, and P. Y. Tzeng, "Hybrid molecular dynamics-continuum simulation for nano/mesoscale channel flows," Microfluid. Nanofluid. **3**, 665 (2007).
[11] I. G. Kevrekidis, C. W. Gear, J. M. Hyman, P. G. Kevrekidis, O. Runborg, and C. Theodoropoulos, "Equation-free, coarse-grained multiscale computation: Enabling microscopic simulations to perform system-level analysis," Commun. Math. Sci. **1**, 715 (2003).
[12] W. Ren and W. E, "Heterogeneous multiscale method for the modeling of complex fluids and micro-fluidics," J. Comput. Phys. **204**, 1 (2005).
[13] W. E, B. Engquist, X. Li, W. Ren, and E. Vanden-Eijnden, "Heterogeneous multiscale methods: A review," Comm. Comp. Phys. **2**, 367 (2007).
[14] M. Reiner, "A mathematical theory of dilatancy," Am. J. Math. **67**, 672 (1945).
[15] J. H. Ferziger and M. Perić, *Computational Methods for Fluid Dynamics* (Springer, Berlin, 2002).
[16] D. Brown and J. H. R. Clarke, "A comparison of constant energy, constant

temperature and constant pressure ensembles in molecular dynamics simulations of atomic liquids," Mol. Phys. **51**, 1243 (1984).
[17]M. P. Allen and D. J. Tildesley, *Computer Simulation of Liquids* (Oxford University Press, Oxford, 1989).
[18]D. J. Evans and G. P. Morriss, "Non-Newtonian molecular dynamics," Comput. Phys. Rep. **1**, 297 (1984).
[19]D. J. Evans and G. Morris, *Statistical Mechanics of Nonequilibrium Liquids* (Cambridge University Press, New York, 2008).
[20]J. Koplik and J. R. Banavar, "Corner flows in the sliding plate problem," Phys. Fluids **7**, 3118 (1995).
[21]N. G. van Kampen, *Stochastic Processes in Physics and Chemistry* (Elsevier, Amsterdam, 2007).
[22]L. D. Landau and E. M. Lifshitz, *Fluid Mechanics* (Addison-Wesley, Reading, MA, 1959).
[23]In the present simulations of fluctuating hydrodynamics, the random noises are included only in the off-diagonal components of the stress tensor T'. That is, we set $T'_{xx}=T'_{yy}=0$ and $T'_{xy}=T'_{yx}=2\eta E'_{xy}+R'_{\mathrm{CFD}xy}$, where the intensity of the random noise is defined by the fluctuation-dissipation theorem as $\langle R'^2_{\mathrm{CFD}xy}\rangle=2\eta kT/(\Delta x^3\Delta t)$.